Tuning the Emission Color of Europium-Containing Ionic Liquid-Crystalline Phases

Erwann Guillet, Daniel Imbert, Rosario Scopelliti, and Jean-Claude G. Bünzli*

Swiss Federal Institute of Technology, Lausanne, Laboratory of Lanthanide Supramolecular Chemistry, BCH 1402, CH-1005 Lausanne, Switzerland

Received May 3, 2004. Revised Manuscript Received June 15, 2004

Luminescent liquid-crystalline phases are produced by introducing trivalent europium salts, EuY_3 (Y = Cl, NO_3, ClO_4, CF_3SO_3), in room-temperature ionic liquids (RTIL) derived from 1-alkyl-3-methylimidazolium, [C_n-mim]X (X = Cl, NO_3; n = 12−18). Four new ionic liquids are synthesized (X = NO_3^-, n = 12, 14, 16, 18) and characterized, and the structure of [C_{12}-mim]Cl is elucidated by X-ray diffraction. Differential scanning calorimetry and polarized light microscopy demonstrate that the liquid-crystalline properties of europium-containing [C_{12}-mim]Cl are not much affected up to a salt concentration of 10 mol %, except for the mesogenic window which is enlarged. The RTIL displays a blue fluorescence and its intensity decreases substantially upon the introduction of Eu^{III} salts, pointing to energy transfer from the RTIL to the metal ion. A high-resolution luminescence study conducted both at room and low (10 K) temperature unambiguously demonstrates that the 5 mol % solutions contain a single solvated Eu^{III} species; when the counterion is Cl^-, ClO_4^-, or $CF_3SO_3^-$, it appears to be a polychloro complex with a low symmetry derived from an idealized cubic symmetry. In the case of nitrate, a stronger anion-Eu^{III} interaction results in an emission spectrum in which the hypersensitive metal-centered red transition ($^5D_0 \rightarrow {}^7F_2$) predominates. As a matter of fact, the emission color of the liquid-crystalline phases can be easily turned from blue to red, depending on the excitation wavelength and the counterion Y, as demonstrated by the trichromatic coordinates of these materials.

Introduction

In the past few years, lanthanide-containing liquid-crystalline (LC) phases have gained increasing interest, particularly in view of their potential photo- and/or electro-luminescent properties. In addition, the large magnetic anisotropy of the lanthanide ions may allow magnetic rather than electric switching of the LC phases.[1] The luminescence of trivalent lanthanides, with narrow−band emission providing a high color purity, appears to be well-suited for the development of novel liquid-crystalline displays (LCDs). Among the lanthanide series, europium is peculiar since both its trivalent and divalent states are luminescent. Therefore, liquid-crystalline materials with switchable luminescence from red Eu^{III} to blue Eu^{II} (and vice versa) can be envisaged if matrixes able to stabilize both oxidation states, and allowing electric switching between them, are found. Macrocyclic receptors are good candidates,[2] but the synthesis of adequate mesogenic or pro-mesogenic receptors is quite involved[3] and the resulting complexes do not always display the desired mesogenic phases.[4]

Recently, Billard et al.[5] have demonstrated that a room-temperature ionic liquid (RTIL), [Bu-mim]PF_6, stabilizes the low oxidation state of europium. RTILs exhibit all the properties of regular salts such as electric conductivity, very low vapor pressure, and, additionally, they possess high solvating properties and they are easy to handle.[6] The solvation of Eu^{III} in RTILs has been investigated using molecular dynamics,[7,8] while its luminescence properties in [Bu-mim]Tf_2N, 1-methyl-3-butylimidazolium bis(trifluoromethanesulfonyl)imide, have been the subject of a recent report.[9] Inspired by previous works which attempted to produce magnetic[10] and/or luminescent[11] liquid-crystalline phases from pyridinium derivatives, particularly hemicyanine salts,[11] our idea was to test if luminescent liquid-crystalline materials could be devised by using mesogenic RTILs.

* To whom correspondence should be addressed. E-mail: jean-claude.bunzli@epfl.ch.

(1) Binnemans, K.; Görller-Walrand, C. *Chem. Rev.* **2002**, *102*, 2303−2345.
(2) Sastri, V. S.; Bünzli, J.-C. G.; Rao, V. R.; Rayudu, G. V. S.; Perumareddi, J. R. *Modern Aspects of Rare Earths and Complexes*; Elsevier B.V.: Amsterdam, 2003; Chapter 4B.
(3) Suarez, S.; Mamula, O.; Imbert, D.; Piguet, C.; Bünzli, J.-C. G. *Chem. Commun.* **2003**, 1226−1227.
(4) Binnemans, K.; Gundogan, B. *J. Rare Earths* **2002**, *20*, 249−255.
(5) Billard, I.; Moutiers, G.; Labet, A.; El Azzi, A.; Gaillard, C.; Mariet, C.; Lützenkirchen, K. *Inorg. Chem.* **2003**, *42*, 1726−1733.
(6) Welton, T. *Chem. Rev.* **1999**, *99*, 2071−2083.
(7) Chaumont, A.; Wipff, G. *Phys. Chem. Chem. Phys.* **2003**, *5*, 3481−3488.
(8) Chaumont, A.; Wipff, G. *J. Phys. Chem. B* **2004**, *108*, 3311−3319.
(9) Billard, I.; Mekki, S.; Gaillard, C.; Hesemann, P.; Moutiers, G.; Mariet, C.; Labet, A.; Bünzli, J.-C. G. *Eur. J. Inorg. Chem.* **2004**, *6*, 1190−1197.
(10) Wang, K. Z.; Huang, C. H.; Xu, G. X.; Zhou, Q. F. *Solid State Commun.* **1995**, *95*, 223−225.
(11) Binnemans, K.; Bex, C.; van Deun, R. *J. Inclusion Phenom. Macrocyclic Chem.* **1999**, *35*, 63−73, and references therein.

10.1021/cm049296o CCC: $27.50
Published on Web 09/25/2004

1-Dodecyl-3-methylimidazolium chloride, [C_{12}-mim]Cl, exhibits a smectic A phase between −2.8 and 104.4 °C,[12] so that as a first step toward the design of switchable luminescent LC phases, we have introduced various europium salts, chloride, nitrate, perchlorate, and trifluoromethanesulfonate, into this RTIL. Both the thermal and luminescence properties of the resulting phases have been studied. In addition, the X-ray structure of [C_{12}-mim]Cl has been determined and we have synthesized new ionic liquids in order to assess the influence of the counterion and of the length of the alkyl chain. The final goal here is to investigate to which extent the emission color of the LC phases can be tuned by varying either their composition or the excitation wavelength.

Experimental Section

All reagents and solvents were used as received (Acros).

Synthesis of the Europium Salts. Europium chloride,[13] perchlorate,[14] nitrate,[14] and triflate[15] were prepared from the oxides (Rhône-Poulenc, 99.99%) and their metal content determined by titration with Titriplex III (Merck) in the presence of urotropine and xylene orange.[16] A sample of elpasolite $Na_2CsEuCl_6$ was also prepared,[17] but revealed to be insoluble in the studied RTILs.

Synthesis of the Ionic Liquids. 1-Dodecyl-3-methylimidazolium chloride ([C_{12}-mim]Cl) was prepared in good yield (over 90%) according to the literature procedure.[12] 1-Alkyl-3-methylimidazolium nitrates ([C_n-mim]NO_3, n = 12, 14, 16, 18) were prepared in good yields (over 80%) from the corresponding chloride salts by reaction with silver nitrate (one detailed example is given below). Absence of chloride was ascertained by adding silver nitrate to an aqueous solution of the targeted compound at 70 °C. NMR spectroscopy indicated that the salts readily absorb atmospheric humidity, up to a content of 0.5 mole per formula weight.

Synthesis of [C_{12}-mim]NO_3. A solution of silver nitrate (233 mg, 1.37 mmol) in water (15 mL) was added to a stirred solution of [C_{12}-mim]Cl·H_2O (410 mg, 1.34 mmol) in CH_2Cl_2 (15 mL). The mixture was centrifuged after 5 min of hefty stirring and the aqueous phase was extracted with CH_2Cl_2 (3 × 15 mL). The organic phase was washed with water (15 mL) and dried over $MgSO_4$ and the solvent was removed under reduced pressure to yield a pale yellow liquid which solidified into a low melting point solid (yield 351 mg, 84%). ^{1}H NMR (400 MHz, $CDCl_3$): δ/ppm 0.86 (3H, t, J = 6.9 Hz, −N(CH_2)$_{11}$CH_3), 1.23−1.30 (18H, m, −(CH_2)$_9$CH_3), 1.87 (2H, m, −NCH_2CH_2−), 4.00 (3H, s, −NCH_3), 4.21 (2H, t, J = 7.3 Hz, −NCH_2−), 7.32 (1H, s, −NC*H*CH−), 7.42 (1H, s, −NCHC*H*−), 9.91 (1H, s, −NC*H*N−). ^{13}C NMR (100 MHz, $CDCl_3$): δ/ppm 14.22 (−*C*H_3), 22.79, 26.40, 29.12, 29.44, 29.52, 29.64, 29.72, 29.73, 30.37, 32.03 −(*C*H_2)$_{10}$CH_3), 36.39 (−N*C*H_3), 50.25 (−N*C*H_2−), 122.35 (−N*C*HCH−), 124.00 (−NCH*C*H), 137.80 (−N*C*HN−). IR (ATR): ν_{max}/cm^{-1} 3462 (O−H), 3099 (s, aromatic C−H stretch), 2919, 2851 (m, aliphatic C−H stretch), 1635 (s), 1572, 1469 (s, symmetric ring stretch), 1345 (NO_3), 1168, 1089, 845, 829, 794, 721, 658. ESI-MS (MeOH): m/z 251.40 ([C_{12}-mim]$^+$, calc. 251.25). Anal. Calcd for $C_{16}H_{31}N_3O_3$: C, 61.3; H, 10.0; N, 13.4. Found: C, 61.6; H, 10.0; N, 13.6.

Elemental analyses for [C_n-mim]NO_3, n = 14, 16, and 18, are given in Table S1 (Supporting Information).

Preparation of Eu-Containing [C_{12}-mim]Cl Solutions. The europium salt was added under nitrogen atmosphere to the melted ionic liquid. Water was then removed by heating at 150 °C in vacuo (10^{-1} Torr). The following notation has been adopted for the samples: a letter stands for the anion (C for chloride, N for nitrate, P for perchlorate, and T for triflate) and the subsequent number gives the molar percentage of the europium salt. The preparation of [C_{12}-mim]Cl containing 5 mol % of $EuCl_3$ (**C5**) is given as a typical example: [C_{12}-mim]Cl·H_2O (290 mg, 0.95 mmol) was introduced into a Schlenk tube under a nitrogen atmosphere and heated at 120 °C until fully molten; $EuCl_3$·5H_2O (17.4 mg, 0.05 mmol) was added to the liquid and the tube was heated under vigorous stirring at 150 °C in vacuo (10^{-1} Torr) until no more water evolved. The full dehydration was attested by thermogravimetric analysis, which revealed that the amount of remaining water is inferior to 0.5% (w/w). Upon cooling, the material solidified into a viscous, pale yellow liquid-crystalline material.

A number of LC phases were prepared with Eu^{III} chloride, nitrate, perchlorate, and triflate, the salt concentrations ranging from 5 to 30 mol %. *Caution! Perchlorate salts combined with organic ligands are potentially explosive and should be handled in small quantity and with the necessary precautions.*

Spectroscopic and Analytical Measurements. ^{1}H and ^{13}C NMR spectra were recorded in $CDCl_3$ solutions with a Bruker Avance DRX400 spectrometer at room temperature. Mid-infrared spectra were recorded using a Perkin-Elmer Spectrum One spectrometer equipped with a Universal Attenuated Total Reflection sampler. Far-infrared spectra were measured on a Bruker IFS 113V FTIR spectrometer using polyethylene windows. DSC thermograms were recorded on a Setaram DSC 131 instrument equipped with a liquid nitrogen cooler. Transition temperatures were determined under a nitrogen atmosphere as follows: the samples were heated from room temperature up to 250 °C at a rate of 10 °C·min^{-1} and held at this temperature for 5 min in order to allow for complete dehydration. Three cooling−heating cycles between 200 and −100 °C were then performed at a rate of 10 °C·min^{-1}. The transition temperatures and enthalpies extracted from the second and subsequent cycles were completely reproducible. Thermogravimetric traces were obtained with a Pyris 6 thermogravimetric analyzer from Perkin-Elmer.

UV−visible spectra were measured with a Lambda 900 spectrometer from Perkin-Elmer using 1-cm quartz cells. The experimental procedures for high-resolution, laser-excited luminescence measurements have been published previously.[18] Continuous spectra were excited with an Coherent Innova-90 dye laser and corrected for the instrumental function as well as for the residual emission of the RTIL. Lifetimes were measured using a Lambda-Physik-FL3002 pulsed dye laser pumped at 532 nm. Luminescence decays of the doped phases were corrected by subtraction of the intrinsic decay of the RTIL; they are averages of at least three independent determinations. Low-resolution excitation and emission spectra were recorded on a Jobin Yvon Horiba Fluorolog FL3-22. The refractive index measurements were performed on an Abbe refractometer from Zeiss operating at room temperature. Samples were under the form of thin films.

Optical analyses were made by heated-stage polarized light microscopy (PLM) with a Leitz-Wetzler microscope equipped with a heated sample holder and temperature controller. The images were recorded with a JVC digital camera during the cooling stage at 80 °C, after initial heating to 120 °C. Heating and cooling rates were 10 °C·min^{-1}.

X-ray Structure of [C_{12}-mim]Cl. Data collection was performed at 140 K on a 4-circle kappa goniometer equipped with an Oxford Diffraction KM4 Sapphire and using graphite

(12) Bradley, A. E.; Hardacre, C.; Holbrey, J. D.; Johnston, S.; McMath, S. E. J.; Nieuwenhuyzen, M. *Chem Mater.* **2002**, *14*, 629−635.
(13) Taylor, M. D.; Carter, C. P. *J. Inorg. Nucl. Chem.* **1962**, *24*, 387−391.
(14) Bünzli, J.-C. G.; Mabillard, C.; Yersin, J.-R. *Inorg. Chem.* **1982**, *21*, 4214−4218.
(15) Bünzli, J.-C. G.; Pilloud, F. *Inorg. Chem.* **1989**, *28*, 2638−2642.
(16) Schwarzenbach, G. *Complexometric Titrations*; Chapman & Hall: London, 1957.
(17) Morss, L. R.; Siegal, M.; Stenger, L.; Edelstein, E. *Inorg. Chem.* **1970**, *9*, 1771−1775.
(18) Rodriguez-Cortinas, R.; Avecilla, F.; Platas-Iglesias, C.; Imbert, D.; Bünzli, J.-C. G.; de Blas, A.; Rodriguez-Blas, T. *Inorg. Chem.* **2002**, *41*, 5336−5349.

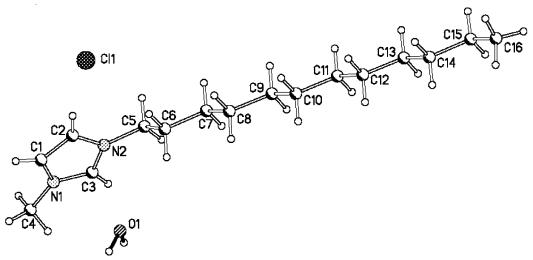

Figure 1. Molecular structure of $[C_{12}\text{-mim}]Cl\cdot H_2O$ showing the atom-numbering scheme.

Table 1. Parameters of the H-Bond Network in $[C_{12}\text{-mim}]Cl\cdot H_2O$

donor-H...acceptor	D−H/Å	H...A/Å	D...A/Å	D−H...A/°
O1−H1A...Cl1	0.98(9)	2.43(11)	3.333(13)	152(15)
O1−H1B...Cl1	0.99(12)	2.30(11)	3.228(13)	155(10)
C2−H2...Cl1	0.95	2.56	3.497(17)	169
C3−H3...O1	0.95	2.30	3.16(2)	152
C1−H1...Cl1		2.86		
C4−H4B...Cl1		2.88		
C4−H4C....Cl1		2.88		

monochromated Mo(Kα) radiation (0.71073 Å). Data reduction was carried out with CrysAlis RED, release 1.7.0.[19] Structure solution and refinement, as well as molecular graphics and geometrical calculations, were performed with release 5.1 of the SHELXTL software package.[20] The structure was refined using full-matrix least-squares on F^2 with all non-H atoms anisotropically defined. H atoms were placed in calculated positions using the "riding model" except those belonging to water, for which a "free" model has been employed. Crystallographic data: triclinic, space group $P\bar{1}$, $a = 5.345(6)$ Å, $b = 7.722(8)$ Å, $c = 22.828(17)$ Å, $\alpha = 84.24(8)°$, $\beta = 84.18(8)°$, $\gamma = 78.44(10)°$, $Z = 2$, 4536 observed reflections of which 2281 were used for the refinement, and $R_f = 0.1609$. Crystallographic supplementary data are in CIF format.

Results

Structure of $[C_{12}\text{-mim}]Cl\cdot H_2O$. Suitable single crystals were obtained at room temperature from a 1,2-dichloroethane solution in contact with atmospheric moisture. They were obtained as transparent thin plates crystallizing in triclinic $P\bar{1}$ space group. The molecular structure along with the atom-numbering scheme are shown in Figure 1. All the distances and angles are standard, and the length of the molecule from the methyl carbon of the imidazole moiety (C4) to the terminal methyl carbon of the chain (C16) is 18.673 Å.

The molecules are connected via an extensive network of hydrogen bonds. The strongest interactions are those linking water molecules and the chloride ions (see Table 1).

Each chloride ion is surrounded by two water molecules and each of the latter interacts with two adjacent anions, generating an infinite one-dimensional chain along the base vector [1 0 0] (*a* axis, see Figure 2 and Figure S2, Supporting Information). A closer look around the chlorides shows some weaker interactions involving the CH and CH_3 groups and ranging from 2.56 up to 2.88 Å (see Table 1). The hydrogen network around each water molecule is completed by a CH...O interaction. In fact, these interactions, along with the interdigitation of the alkyl chain, create alternating lipophilic (nonpolar) and hydrophilic (polar) domains in the structure. The interplanar distance is equal to the lattice *a* parameter, 5.345(6) Å, and the distance between the chains is given by $b/2 = 3.861(8)$ Å (see Figure S1, Supporting Information). The distance between two consecutive rings (from N2 to N2) is 4.1 Å. A previous SAXS study performed on both the crystalline and liquid-crystalline state of $[C_{12}\text{-mim}]Cl$ revealed a *d* spacing of 22.5 and 31.7 Å, respectively.[12] Our measurement stays in line with this as the *c* parameter is equal to 22.83(2) Å. Moreover, the emerging picture is coherent with the conclusions drawn by Downard et al. who recently reported the crystal structure of $[C_{14}\text{-mim}]Cl$ and $[C_{18}\text{-mim}]Cl$, in which strong hydrogen bonds form O−H...Cl chains.[21]

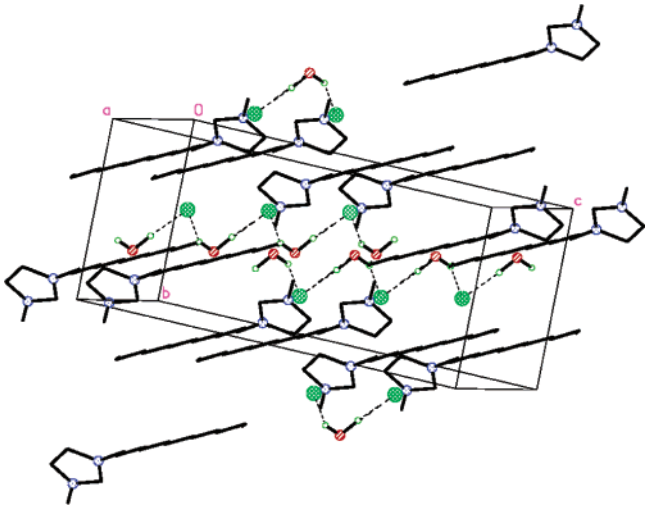

Figure 2. Schematic representation of the hydrogen bond network between water and chloride ions in the structure of $[C_{12}\text{-mim}]Cl\cdot H_2O$.

Mesogenic Properties. The mesogenic properties of the $[C_n\text{-mim}]Cl$ series have been reported,[12] and we have investigated the effect generated by the replacement of the chloride ion by nitrate. This was motivated by the fact that nitrate ions, which are more coordinating than chloride ions, are known to enhance the luminescence properties of Eu^{III} in protic and polar solvents.[22] The parameters characterizing the mesogenic behavior of $[C_n\text{-mim}]NO_3$ ($n = 12$, 14, 16, 18), namely, transition temperatures and enthalpies, are reported in Table 2. The three salts with $n = 14$, 16, and 18 exhibit ionic liquid-crystalline phases appearing above room temperature, in the range 47−64 °C. The mesogenic window is large, increasing from 80 °C for $n = 14$ to 130 and 150 °C for $n = 16$ and 18, respectively. This behavior parallels the one of the chloride salts for which the $Cr-Sm_A$ transition temperature increases from −2.8 ($n = 12$) to 53.2 ($n = 18$) °C, while the isotropization temperature augments from 104.4 ($n = 12$) to 204 ($n = 16$) °C.[12] Although the mesogenic properties of the nitrates are interesting per se, they do not match our

(19) CrysAlis RED, release 1.7.0; Oxford Diffraction Ltd.: Abingdon, Oxfordshire, UK, 2003.
(20) Sheldrick, G. M. SHELXTL; University of Göttingen: Göttingen, Germany, 1997; Bruker AXS, Inc., Madison, WI.
(21) Downard, A.; Earle, M. J.; Hardacre, C.; McMath, S. E. J.; Nieuwenhuyzen, M.; Teat, S. J. *Chem. Mater.* **2004**, *16*, 43−48.
(22) Bünzli, J.-C. G.; Milicic-Tang, A. In *Handbook on the Physics and Chemistry of Rare Earths*; Gschneidner, K. A., Jr., Eyring, L., Eds.; Elsevier Science Publ. B.V.: Amsterdam, 1995; Vol. 21, Chapter 145.

Table 2. Transition Temperatures (± 0.5 °C) and Enthalpies (± 5%) of [C_n-mim]NO_3 Salts, as Determined from DSC Experiments after an Initial Heating at 250 °C To Ensure That the Samples Are Perfectly Anhydrous

		heating		cooling	
n	transition	*T*/ °C	Δ*H*/kJ mol^{-1}	*T*/°C	Δ*H*/kJ mol^{-1}
12	Cr-I	39.5	25.1	18.3	−23.0
14	Cr-LC	47.4	29.2	35.9	−24.2
	LC-I	126.6	0.05	129.0	−0.05
16	Cr-LC	52.5	31.8	40.6	−25.5
	LC-I	182.7	0.8	184.2	−0.8
18	Cr-LC	64.0	33.4	53.9	−27.7
	LC-I	213.4	1.0	216.0	−0.9

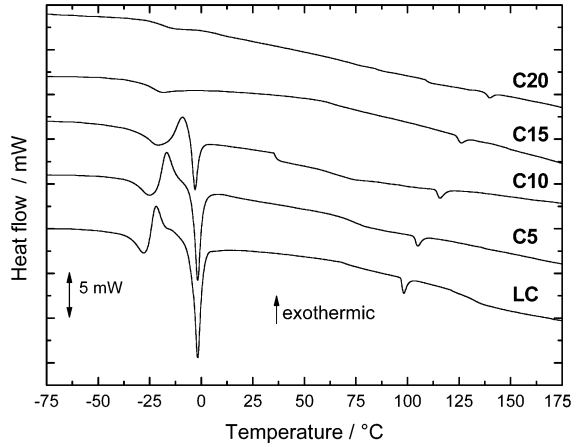

Figure 3. DSC heating traces of [C_{12}-mim]Cl and [C_{12}-mim]-Cl doped with $EuCl_3$ at 5 (**C5**), 10 (**C10**), 15 (**C15**), and 20 (**C20**) mol %.

needs for room-temperature liquid-crystalline phases and, therefore, we have turned to [C_{12}-mim]Cl only for producing room-temperature, lanthanide-doped liquid-crystalline phases.

In an initial set of experiments, [C_{12}-mim]Cl has been doped with 5 (**C5**), 10 (**C10**), 15 (**C15**), and 20 (**C20**) mol % of europium chloride and DSC thermograms of the resulting compounds have been recorded after an initial dehydration step (Figure 3). The overall shapes of the thermograms remain very similar up to a doping rate of 10 mol %. One notes that the temperature of the Cr-LC phase transition slightly decreases, while the temperature of the LC-I transition increases by about 20 °C. As a result, the mesogenic window is enlarged (Figure S3, Supporting Information). A concentration larger than 10 mol % results in considerable changes in the thermograms, particularly with respect to the enthalpies of transition. The main feature around 0 °C disappears, but the trend in the isotropization temperature observed for the smaller concentrations is maintained.

The same experiments have been conducted with the other europium salts, nitrate, perchlorate, and triflate. A behavior similar to that of [C_{12}-mim]Cl is observed for the concentration dependence of the mesogenic properties so that transition temperatures are reported at a concentration of 10 mol % only in Table 3. The addition of nitrate does not affect much the thermal properties of [C_{12}-mim]Cl; it simply increases the metastability range of the liquid-crystalline phase upon cooling. The latter observation also holds for perchlorate and triflate, but for these salts we note two differences:

Table 3. Transition Temperatures (in °C, ± 0.5 °C) from DSC Thermograms for [C_{12}-mim]Cl Doped with 10 Mol % of EuX_3; Data from Heating and Cooling Steps after Dehydration of the Compounds

X^-	Cr-LC	LC-I	I-LC	LC-Cr
no Eu(III)	−7.8	96.5	99.2	−5.6
Cl^-	−8.4	113.4	114.8	−7.4
NO_3^-	−9.0	95.0	101.0	−19.3
ClO_4^-	−8.2	85.0[a,b] 93.3[b]	91.1[a,b] 95.8[b]	−17.9
$CF_3SO_3^-$	−8.9	75.0[a,b] 99.5[b]	81.4[a,b] 90.0[b]	−14.9

[a] LC-LC transition. [b] ± 1.5 °C.

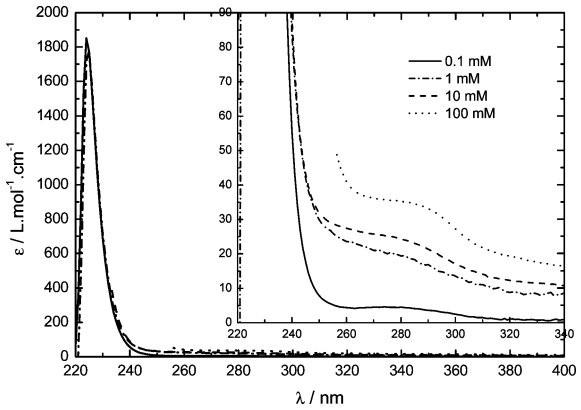

Figure 4. Absorption spectra of [C_{12}-mim]Cl solutions in CH_2-Cl_2.

(i) a LC-LC transition takes place at 5 and 25 °C before isotropization for ClO_4^- and $CF_3SO_3^-$, respectively, and (ii) the mesogenic windows are narrowed with respect to the pure [C_{12}-mim]Cl sample.

The nature of the Eu^{III}-containing mesogenic phases has been investigated by polarized light microscopy. The images obtained for [C_{12}-mim]Cl, **C10**, and **P10** are very similar (Figure S4, Supporting Information) so that the liquid-crystalline phases evidenced in our materials are most probably smectic A phases, as reported for [C_{12}-mim]Cl.[12] Further experiments involving small-angle X-ray scattering are ongoing in order to fully characterize these phases.

Optical Properties of Pure [C_{12}-mim]Cl. UV−visible absorption spectra of [C_{12}-mim]Cl solutions at different concentrations in dichloromethane are given in Figure 4. The spectra feature two absorption bands, one centered at 224 nm with $\epsilon = 1800$ M^{-1}·cm^{-1} and a second one at 280 nm, weaker and broader. The molar absorption coefficient of the latter depends on the concentration, ranging from about 5 M^{-1}·cm^{-1} at 0.1 mM up to 35 M^{-1}·cm^{-1} at 0.1 M. This indicates the formation of a new species, via intermolecular interactions taking place in solution.

The excitation spectra of the dichloromethane solutions confirm this observation, with a main excitation maximum at 274 nm and a very small component at 344 nm, the contribution of which grows with increasing concentration. Emission occurs at 410 nm and the broad luminescence band undergoes a slight shift to 400 nm as the concentration increases.

The excitation and emission spectra of a pure sample of [C_{12}-mim]Cl are similar to the spectra measured for the 1 M solution, except for a growing importance of

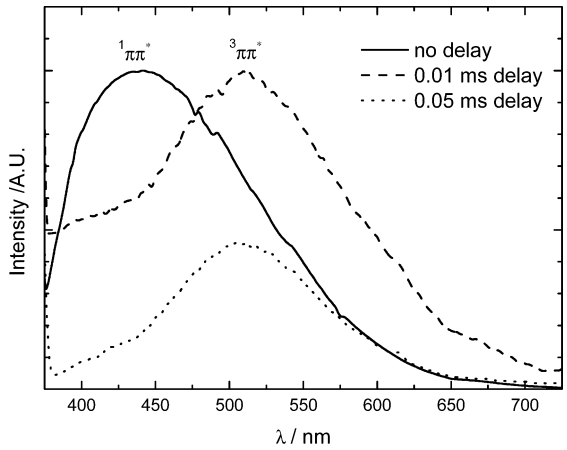

Figure 5. Normalized emission spectra of frozen [C_{12}-mim]-Cl (77 K, excitation at 370 nm) showing the disappearance of the $^1\pi\pi^*$ fluorescence when a time delay is enforced.

the shoulder at 344 nm (see Figure S5, Supporting Information). This emission disappears as soon as a time delay is enforced so that it is easily assigned as arising from a singlet state. Upon freezing of the pure [C_{12}-mim]-Cl sample down to 77 K, another weak and broad emission band is detected with a maximum at 510 nm that we tentatively assign to emission from $^3\pi\pi^*$ states (Figure 5). Time-resolved luminescence however shows that the intensity decay of this emission cannot be fitted with a single exponential, nor with poly-exponential, functions. The intensity decays initially relatively fast but then trails as if re-population of the excited states were occurring (possibly through reabsorption and/or the formation of an excimer). Investigation of the $EuCl_3$-doped materials (vide infra) also showed the presence of a residual intensity at 612 nm arising from a long-lived RTIL emission, even at room temperature. Again, the decay is nonexponential, but an approximate lifetime of 100 ms could be estimated (see Figure S6, Supporting Information). For this reason, the luminescence decays measured on Eu^{III}-containing materials have been corrected by subtracting the residual luminescence of [C_{12}-mim]Cl. In this way, perfectly exponential decays were obtained.

Optical Properties of the Europium-Containing LC Phases. The absorption spectra of solutions of **C5** and **N5** in dichloromethane are reported in Figure 6. The band centered at 280 nm appears to be enhanced upon addition of the lanthanide salts, particularly in the case of chloride. In addition, the spectrum of **C5** displays a third absorption band at 295 nm, with a molar absorption coefficient equal to 280 $M^{-1}\cdot cm^{-1}$. It is noteworthy that this transition is also observed when tetrabutylammonium chloride (TBACl) is added to a dichloromethane solution containing 5 mol % of $EuCl_3$. Therefore, we assign it to a chloride-to-Eu^{III} charge transfer state, consecutive to the formation of a polychloro species. Similar states have been observed at 31 200 cm^{-1} for $EuCl_3$ solutions in [Bu-mim]Tf_2N containing TBACl,[9] and at 33 200 cm^{-1} ($\epsilon = 400\ M^{-1}\cdot cm^{-1}$) for $[EuCl_6]^{3-}$ in acetonitrile saturated with Et_4NCl.[23]

The excitation spectra of **C5** and **N5** (Figure S7, Supporting Information) display two broad bands arising from the RTIL, at 274 and 335 nm, pointing to energy transfer from the ionic liquid to the Eu^{III} ion. In addition, several discrete and weak f−f transitions can be identified at 361 nm ($^5D_4 \leftarrow {}^7F_0$), 375 nm ($^5G_J \leftarrow {}^7F_{0/1}$), 380 nm ($^5L_7, ^5G_J \leftarrow {}^7F_{0/1}$), 393 nm ($^5L_6 \leftarrow {}^7F_0$), 400 nm ($^5L_6 \leftarrow {}^7F_1$), 415 nm ($^5D_3 \leftarrow {}^7F_0$), 464 nm ($^5D_2 \leftarrow {}^7F_0$), 525 nm ($^5D_1 \leftarrow {}^7F_0$), and 534 nm ($^5D_1 \leftarrow {}^7F_1$). The intensity of these f−f excitation bands is larger in the case of the material containing europium nitrate, for which the most efficient excitation wavelength lies at 393 nm. The excitation spectra of the **P5** and **T5** samples display the same features as **C5**, i.e., the two broad bands of the RTIL and the weaker f−f transitions, the latter being 10−15% less intense than that for **C5**.

Emission spectra obtained upon excitation into the most energetic excitation band of the ionic liquid still display emission from [C_{12}-mim]Cl. Its intensity is however drastically decreased compared to pure [C_{12}-mim]Cl, by a factor up to 15 for **C5** for instance (Figure 7). This clearly confirms that energy transfer occurs from the RTIL to the metal ion. In addition, all the doped phases exhibit the characteristic metal-centered $^5D_0 \rightarrow {}^7F_J$ emission bands, located at 580, 591, 611, 661, and 702 nm for $J = 0$, 1, 2, 3, and 4, respectively.

For **C5**, the intensity ratio of the hypersensitive $^5D_0 \rightarrow {}^7F_2$ transition to the magnetic dipole transition

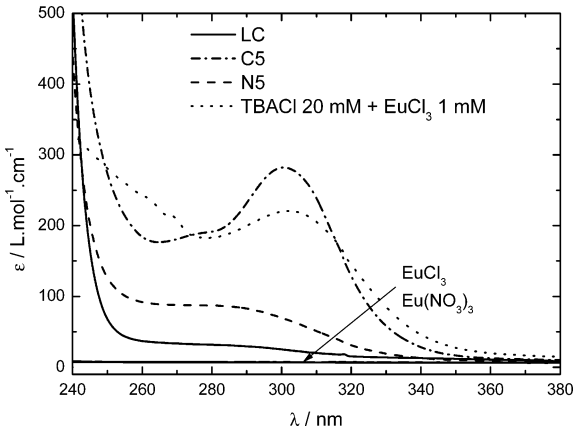

Figure 6. Absorption spectra of dichloromethane solutions of 20 mM [C_{12}-mim]Cl, 20 mM **C5**, 20 mM **N5**, and 20 mM Eu-containing TBACl and of the Eu^{III} salts at 1 mM, for comparison reasons.

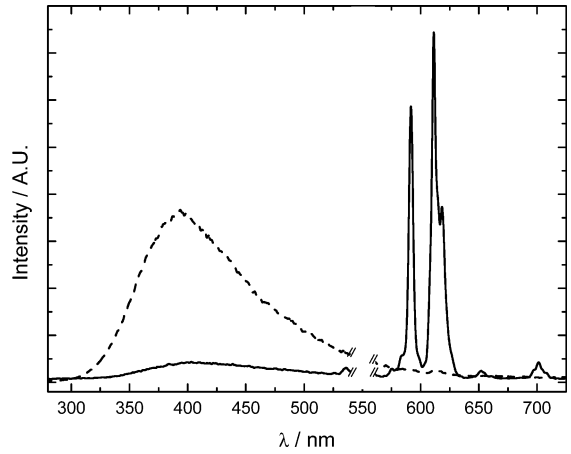

Figure 7. Part of the emission spectra of [C_{12}-mim]Cl (dash) and **C5** (line) obtained at room temperature (mesogenic phases) under broad band excitation at 274 nm. Rayleigh bands are suppressed.

(23) Ryan, J. L.; Jørgensen, C. K. *J. Phys. Chem.* **1966**, *70*, 2845−2857.

Table 4. Intensity Ratios $I(^5D_0 \rightarrow {}^7F_2)/I(^5D_0 \rightarrow {}^7F_1)$, Lifetimes, Refractive Indices, and Intrinsic Eu^{III} Quantum Yields for C5, N5, P5, T5 (LC phases) and for a Solid State Sample of Elpasolite ($Cs_2NaEuCl_6$), at Room Temperature

	$I(^7F_2)/I(^7F_1)$	τ_{obs}/ms	n	$Q^a \pm 2\%$
C5	2.9	2.81 ± 0.06	1.5059	61%
N5	4.8	1.58 ± 0.04	1.5014	52%
P5	2.9	2.80 ± 0.03	1.4988	59%
T5	3.2	2.18 ± 0.07	1.4985	52%
elpasolite	1.4	3.54 ± 0.02		

[a] Calculated from high-resolution experiments.

$^5D_0 \rightarrow {}^7F_1$ is clearly larger than 1, ruling out the presence of an octahedral hexachloro species (Table 4). The emission spectra of **P5** and **T5** present the same patterns and intensity ratios, so it can be inferred that the resulting solvated species are very similar when europium chloride, perchlorate, or triflate are introduced into [C_{12}-mim]Cl. Indeed, triflate and perchlorate are known to be labile and weakly coordinating anions,[24] and in the presence of an excess of chloride anions arising from the RTIL, a polychloro environment similar to the one in **C5** forms.

The overall shape of the emission spectra of $EuCl_3$ solutions in the mesogenic phase of [C_{12}-mim]Cl remains similar with increasing concentration (Figure S8, Supporting Information), while the intensity of the hypersensitive transition increases linearly up to 25 mol %. For a larger concentration, the intensity decreases again, probably due to an internal filter effect. Taking into account the thermal properties discussed above, the subsequent studies have therefore been restricted to samples with concentrations lower than 10 mol %, typically equal to 5 mol %.

Sample **N5** exhibits a rather different luminescence spectrum, compared with **C5**, **P5**, and **T5**, especially with respect to the shape and intensity of the $^5D_0 \rightarrow {}^7F_2$ transition. Therefore, a different solvated species exists in this solution, as a consequence of the stronger donor properties of the nitrate ions which effectively compete with chloride ion for inner-sphere binding.

All the corrected luminescence decays, measured under selective excitation on the $^5L_6 \leftarrow {}^7F_0$ transition of europium at 393 nm, turned out to be single-exponential functions and the corresponding lifetimes confirm the existence of the two different solvated species evidenced above for **C5**, **P5**, and **T5** on one hand, and **N5** on the other hand (Table 4). Samples **C5** and **P5** display the same, long lifetime (2.8 ms) characteristic of a metal-ion environment deprived of water molecules. The lifetime exhibited by **T5** is somewhat shorter while the intensity of the hypersensitive transition relative to $^5D_0 \rightarrow {}^7F_1$ is larger; this may reflect some interaction with the triflate anion which is somewhat more coordinating than perchlorate.[24] On the other hand, the luminescence lifetime of **N5** is much shorter and close to the reported lifetime for an anhydrous solution of europium nitrate in acetonitrile (1.35 ms),[25] in line with a strong interaction between Eu^{III} and nitrate. Similar lifetimes are obtained upon excitation through the RTIL levels (e.g., at 335 nm), but in this case, the intensity profile of the Eu^{III}-containing materials displays the population time of the $Eu(^5D_0)$ level which can be estimated to be about 50 μs (see Figure S9, Supporting Information). This is definite proof for sensitization of the Eu^{III} luminescence by the RTIL.

Finally, to better quantify the luminescence potential of these materials, we have estimated the intrinsic quantum yield of the europium-centered emission, Q_{Eu}, from the observed lifetime, τ_{obs}, and the radiative lifetime, τ_R:[26]

$$Q_{Eu} = \frac{\tau_{obs}}{\tau_R} = \tau_{obs} \cdot A_{MD,0} \cdot n^3 \cdot \left(\frac{I_{tot}}{I_{MD,0}}\right)$$

In the specific case of Eu^{III}, the magnetic dipole $^5D_0 \rightarrow {}^7F_1$ transition has a constant dipolar strength, regardless of the chemical environment of the metal ion and the radiative lifetime can be calculated from the above expression, where $A_{MD,0} = 14.65\ s^{-1}$ is the constant spontaneous emission probability, n the refractive index, I_{tot} the total area of the emission spectrum ($^5D_0 \rightarrow {}^7F_J$, for $J = 0-6$), and $I_{MD,0}$ the $^5D_0 \rightarrow {}^7F_1$ band area. The data reported in Table 4 point to intrinsic quantum yields being rather similar and high so that the different emission properties observed upon excitation into the RTIL levels are to be traced back to variations in light absorption and efficacy of energy transfer.

High-Resolution Luminescence Study of C5 and N5. In the absence of X-ray structural data, a high-resolution luminescence investigation was performed on these two samples in order to obtain more information on the composition and structure of the inner coordination sphere and to unravel whether several different species are in equilibrium.

The excitation spectrum of **C5** recorded in the range of the $^5D_0 \leftarrow {}^7F_{0,1}$ transitions upon monitoring the $^5D_0 \rightarrow {}^7F_2$ transition at room temperature displays the electronic 0-phonon $^5D_0 \leftarrow {}^7F_0$ transition as a weak, narrow, and symmetric feature at 17 244 cm^{-1}, while the $^5D_0 \leftarrow {}^7F_1$ transition occurs at 16 885 cm^{-1} (Figure S10, Supporting Information). The 0−0 transition is accompanied by two vibronic sidebands at higher (Stokes) and lower energy (anti Stokes), with energy differences of 120 and 198 cm^{-1}. Unambiguous assignment of these vibronic transitions is demonstrated by the disappearance of the anti-Stokes components at 77 K and the observation of two vibrations in the IR spectrum at 113 and 189 cm^{-1} (Figure 8). Moreover, excitation on any of these vibronic levels gives an emission spectrum identical to the one recorded by excitation on the 0−0 transition. The uniqueness of the $^5D_0 \leftarrow {}^7F_0$ transition indicates the presence of only one chemical environment for the Eu^{III} ion in the LC phase (see Figure S11, Supporting Information).

At room temperature, the high-resolution emission spectrum of **C5** seems to be indicative of a species with high symmetry since only one component is observed for the $^5D_0 \rightarrow {}^7F_1$ transition (as in the excitation spectrum), which in principle points to an icosahedral or cubic symmetry.[25] On the other hand, the $^5D_0 \rightarrow {}^7F_2$ transition displays features incompatible with this

(24) Bünzli, J.-C. G.; Merbach, A. E.; Nielson, R. M. *Inorg. Chim. Acta* **1987**, *139*, 151−152.

(25) Bünzli, J.-C. G. In *Lanthanide Probes in Life, Chemical and Earth Sciences; Theory and Practice*; Bünzli, J.-C. G., Choppin, G. R., Eds.; Elsevier: Amsterdam, 1989; Chapter 7.

(26) Werts, M. H. V.; Jukes, R. T. F.; Verhoeven, J. W. *Phys. Chem. Chem. Phys.* **2002**, *4*, 1542−1548.

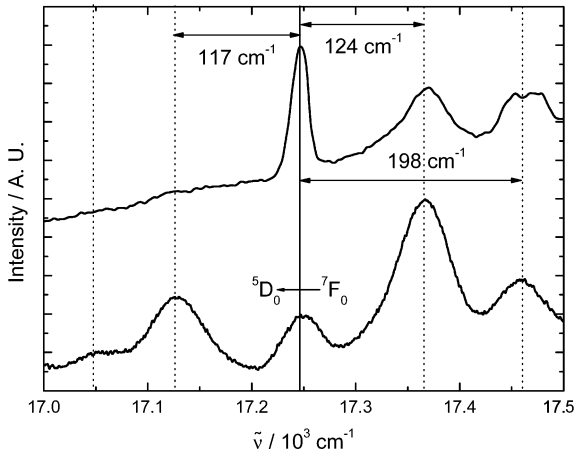

Figure 8. Excitation spectrum of **C5** recorded at 295 K (bottom) and 77 K (top) under medium resolution, while monitoring the $^5D_0 \rightarrow {}^7F_2$ transition at 16 353 cm^{-1}.

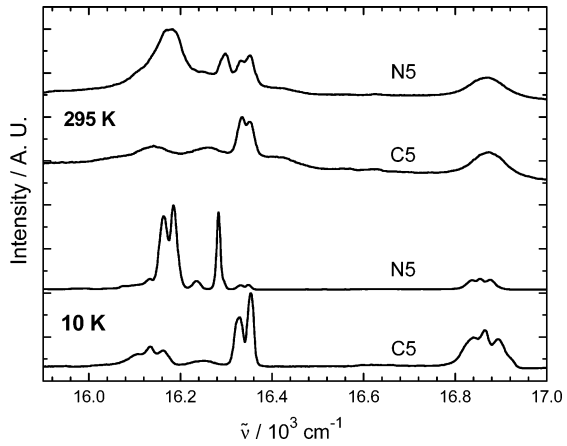

Figure 9. High-resolution emission spectra (excitation on the $^5D_0 \leftarrow {}^7F_0$ transition) of **C5** and **N5** at room temperature and at 10 K.

interpretation since, within such a symmetry, it should either not be observed or yield only one component (in T or T_d symmetries).[25] In our case, the transition to $^7F_2$ is comprised of several vibronic components (839 and 1172 cm^{-1}) associated with the $^5D_0 \rightarrow {}^7F_0$ transition (see Figure S12, Supporting Information). This apparent contradiction can be solved by examining the low-temperature spectra recorded at 10 K (Figure 9): the $^5D_0 \rightarrow {}^7F_1$ transition is now split into three equally spaced components corresponding to a total crystal field effect of 57 cm^{-1}, the sublevels being located at 346, 378, and 403 cm^{-1}. Transitions to the components of $^7F_2$ at 839 and 1172 cm^{-1} disappear, attesting their vibronic origin, and the total crystal-field splitting for this transition (Table S2, Supporting Information) amounts to 247 cm^{-1} (with sublevels at 888, 913, 990, 1077, 1108, and 1135 cm^{-1}). As a comparison, in octahedral elpasolite the $T_{1g}(^7F_1)$ sublevel has been located at 352 cm^{-1} and the (vibronic) E_g and T_{2g} sublevels of $^7F_2$ at 869 and 1082 cm^{-1}, respectively.[27] In conclusion, this high-resolution study points to the LC phase containing only one polychloro species, with low symmetry, arising from a slightly distorted species with idealized cubic symmetry, in view of the weakness of the crystal field effect. The absence of an inversion center is ascertained by $I(^7F_2)/I(^7F_1)$ being much larger than 1.

The excitation spectrum of **N5** is very similar to the one of **C5**, with one symmetrical band for the 0−0 transition occurring at 17 250 cm^{-1} at room temperature, pointing again to only one Eu-containing species in the LC phase (unless a second species with an inversion center is present, which does not seem to be probable in view of the preceding discussion). The corresponding emission spectrum is typical of a species with low symmetry, but differing from the situation found in **C5**, as exemplified in Figure 9. In particular, the $I(^7F_2)/I(^7F_1)$ ratio is much larger (by 65%), indicating a stronger coupling between the anion and Eu^{III}. On the other hand, the overall splittings of the $^5D_0 \rightarrow {}^7F_{1,2}$ transitions are also quite small, about 50 and 201 cm^{-1}, respectively, which is often the case for a highly symmetrical species.

High-resolution emission spectra at room temperature are in line with the already mentioned trend: **C5**, **P5**, and **T5** spectra can practically be superimposed whereas **N5** displays a rather different profile (see Figure S13, Supporting Information). This points to the presence of a common species in **C5**, **P5**, and **T5**.

Chromaticity Diagram. To compare the emissive properties of the liquid-crystalline materials prepared, their color coordinates on the CIE chromaticity diagram have been calculated.[28] In the latter, the chromaticity coordinates of a color, x and y, are calculated as follows:

$$x = \frac{X}{X+Y+Z} \qquad y = \frac{Y}{X+Y+Z}$$

in which X, Y, and Z are the tri-stimulus values:

$$X = \frac{1}{K}\int_{380}^{780} P(\lambda)\cdot\rho(\lambda)\cdot\bar{x}(\lambda)\cdot d\lambda$$

$$Y = \frac{1}{K}\int_{380}^{780} P(\lambda)\cdot\rho(\lambda)\cdot\bar{y}(\lambda)\cdot d\lambda$$

$$Z = \frac{1}{K}\int_{380}^{780} P(\lambda)\cdot\rho(\lambda)\cdot\bar{z}(\lambda)\cdot d\lambda$$

with

$$K = \int_{380}^{780} P(\lambda)\cdot\rho(\lambda)\cdot\bar{y}(\lambda)\cdot d\lambda$$

$P(\lambda)$ is the spectral power distribution of the emitting source, $\rho(\lambda)$ is its spectral reflectance, and $\bar{x}(\lambda)$, $\bar{y}(\lambda)$, and $\bar{z}(\lambda)$ are the CIE spectral trichromatic stimuli taking into account the human physiological response to light. These spectral trichromatic stimuli are tabulated for viewing fields of 2° and 10°. According to these equations, and using the values for a field of 2°, it has been possible to associate two chromaticity coordinates to each of the samples excited at different wavelengths.[29]

Since the overall emission of a typical sample is comprised of the blue contribution from the host RTIL and of the red emission of the europium ion, its color coordinates will be found on a line joining the bluish

(27) Flint, C. D.; Stewart-Darling, F. L. *Mol. Phys.* **1981**, *44*, 61−68.

(28) Narisada, K.; Kanaya, S. In *Phosphor Handbook*; Shionoya, S., Yen, W. M., Eds.; CRC Press Inc.: Boca Raton, FL, 1999; Chapter 17.

(29) http://www.biyee.net/v/cie_diagrams/.

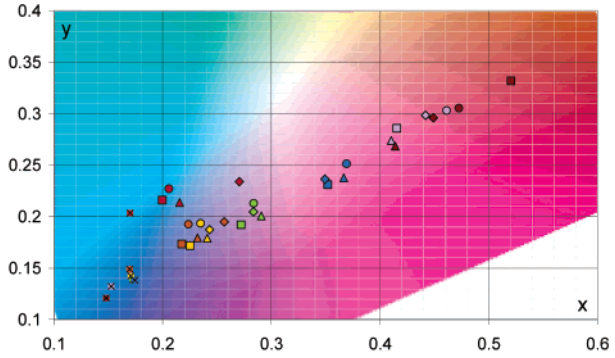

Figure 10. Trichromatic diagram displaying the position of the studied samples in function of their composition (×, LC; ■, C5; ◆, N5; ▲, T5; ●, P5) and the excitation wavelength (gray, 274 nm; violet, 285 nm; blue, 334 nm; green, 344 nm; yellow, 353 nm; orange, 361 nm; red, 393 nm).

section of the diagram to the reddish one. Depending on the excitation wavelength, either the blue or the red component will dominate the emission spectrum. Figure 10 shows how the emission color of the investigated samples depends on both the excitation wavelength and the counterion. For instance, when the **C5**, **P5**, or **T5** samples are excited with a highly energetic wavelength (274 or 285 nm), the energy transfer from the RTIL onto the europium ion is very good, resulting in an almost purely red emission. However, when this material is irradiated with a less energetic wavelength (393 nm), the transfer is less important and the emission is almost purely blue. When the chosen wavelength lies between these limits, the resulting color is purple. On the other hand, for **N5**, excitation at 393 nm yields a rather high red-containing emission because of a direct excitation on the metal center (see its excitation spectrum, Figure S7, Supporting Information).

Conclusions

In this paper, we prove the ability of the room-temperature ionic liquid and liquid-crystalline [C_{12}-mim]Cl to dissolve luminescent europium salts. No dramatic changes in its mesogenic behavior are observed provided the quantity of added salt remains smaller than 10 mol %. Luminescence properties of the europium salts are improved by energy transfer from the RTIL to the metal center. For all the LC phases containing 5 mol % of Eu^{III}, two series of experimental data clearly indicate that only one species forms in solution: solely one $^5D_0 \leftarrow {}^7F_0$ transition is detected and the luminescence decays are single-exponential functions. In the $EuCl_3$-containing sample, formation of a polychloro species is ascertained by the apparition of a charge-transfer band in the absorption spectrum at 33 900 cm^{-1}. However, the intensity ratio $I(^7F_2)/I(^7F_1)$ is clearly much larger than 1, indicating that the emitting species has a distorted geometry with respect to an idealized cubic symmetry. Luminescence spectra, lifetimes, and quantum yields determined on the corresponding samples having perchlorate or triflate as counterion lead to the conclusion that a similar species is present in the LC phases, contrary to nitrate for which a single, but substantially different species is observed.

Another important point is the easy tuning of the luminescent characteristics of the mesogenic phases, from blue to red, by a careful choice of either the excitation wavelength or of the counterion. This paves the way for the use of this type of room-temperature ionic liquid having mesogenic properties for the development of potentially useful luminescent liquid-crystalline materials.

Acknowledgment. This work is supported by the Swiss National Science Foundation (NRP 47). The authors thank Frédéric Gumy for his help in gathering the luminescence data, Daniel Baumann for recording the FTIR spectra, Dr. Kurt Schenk for the use of the polarized light microscope, and Dr. David C. Gross (Osram Sylvania) for sending us the spreadsheet, allowing easy computation of the chromaticity coordinates.

Supporting Information Available: Additonal figures and tables (PDF) and crystallographic details (CIF). This material is available free of charge via the Internet at http://pubs.acs.org.

CM049296O